

X-ray induced photoconductivity and its correlation with structural and chemical defects in heteroepitaxial diamond








Theodor Grünwald, Christina Bestele, Maximilian Bosak, J. Zhao, M. E. Newton, Matthias Schreck


Angaben zur Veröffentlichung / Publication details:

Grünwald, Theodor, Christina Bestele, Maximilian Bosak, J. Zhao, M. E. Newton, and Matthias Schreck. 2023. "X-ray induced photoconductivity and its correlation with structural and chemical defects in heteroepitaxial diamond." *Journal of Applied Physics* 134 (13): 135106. <https://doi.org/10.1063/5.0167532>.

RESEARCH ARTICLE | OCTOBER 04 2023

X-ray induced photoconductivity and its correlation with structural and chemical defects in heteroepitaxial diamond

T. Grünwald ; C. Bestele ; M. Bosak ; J. Zhao ; M. E. Newton ; M. Schreck  

 Check for updates

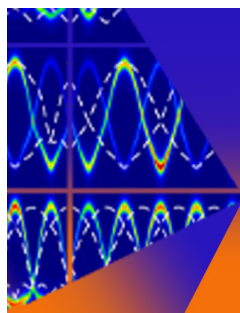
J. Appl. Phys. 134, 135106 (2023)

<https://doi.org/10.1063/5.0167532>


View
Online


Export
Citation

CrossMark



Journal of Applied Physics

Special Topic:
Thermal Transport in 2D Materials

Submit Today

 AIP
Publishing

X-ray induced photoconductivity and its correlation with structural and chemical defects in heteroepitaxial diamond

Cite as: J. Appl. Phys. **134**, 135106 (2023); doi: [10.1063/5.0167532](https://doi.org/10.1063/5.0167532)

Submitted: 13 July 2023 · Accepted: 17 September 2023 ·

Published Online: 4 October 2023



T. Grünwald,¹ C. Bestele,¹ M. Bosak,¹ J. Zhao,² M. E. Newton,² and M. Schreck^{1,a)}

AFFILIATIONS

¹Institut für Physik, Universität Augsburg, D-86135 Augsburg, Germany

²Department of Physics, University of Warwick, Coventry CV4 7AL, United Kingdom

^{a)}Author to whom correspondence should be addressed: matthias.schreck@physik.uni-augsburg.de

ABSTRACT

Three sets of heteroepitaxial diamond crystals grown under nominally identical process conditions on Ir/YSZ/Si(001) substrates have been studied with respect to structural defects, chemical purity, and x-ray induced photoconductivity (PC). The dislocation density that varied systematically between 10^7 and 10^9 cm⁻² had a minor influence on dark conductivity and photoconductive gain G . In contrast, the substitutional nitrogen (N_N) and substitutional boron (N_B) defects, which are both present at very low concentrations (≤ 1 ppb), turned out to be the crucial factors controlling the electrical behavior. Small differences between both resulted in variations of the photocurrents by up to 5 orders of magnitude. The maximum in G of 0.75×10^4 was measured in the sample with highest dark conductivity. It could be explained conclusively within our model calculations on gain formation by $N_N \leq N_B$. For low gain samples, we found $N_N > N_B$. However, the measured G values were far from theoretical predictions. This indicates a dominating role of additional traps. After x-ray switch-off, persistent photoconductivity (PPC) was observed in high gain samples. It was attributed to an energetic barrier hampering the recharging of nitrogen atoms by hole capture. As a possible source, strain fields generated by dislocations are suggested.

© 2023 Author(s). All article content, except where otherwise noted, is licensed under a Creative Commons Attribution (CC BY) license (<http://creativecommons.org/licenses/by/4.0/>). <https://doi.org/10.1063/5.0167532>

I. INTRODUCTION

Diamond is a material with unique physical properties that qualify it for ultimate solutions in mechanical, optical, and electronic applications.¹ In the meantime, polycrystalline and single crystal diamond samples can be synthesized by chemical vapor deposition (CVD), which surpass all the natural crystals in terms of purity and various physical properties. As a consequence, an increasing number of CVD diamond products are entering the market.² In the field of electronics, which includes high power transistors and switches or detectors for ionizing radiation, diamond single crystals of high structural quality and chemical purity are required. While synthesis by homoepitaxy on high pressure high temperature (HPHT) seeds may be a viable option in the field of research and development, production of marketable products needs large area substrates. Freestanding wafers with a maximum diameter of 92 mm have recently become available via heteroepitaxy on Ir/YSZ/Si(001).³ Their structural quality and size are

already satisfactory for commercial applications in cutting tools or as infrared optical elements. In contrast, their potential for electronic devices is still unclear.

To tackle this problem, it is necessary to explore the influence of the most relevant structural and chemical defects in state-of-the-art heteroepitaxial diamond crystals on their electronic properties. In a recent work,⁴ a transient current technique (TCT) had been applied to measure charge collections efficiency (CCE) values, separately for holes and electrons, on two sets of samples exhibiting systematic variations in dislocation density n_{dis} . Pronounced correlations with n_{dis} had been found specifically for electrons, which facilitated derivation of the corresponding capture cross sections.

In the present work, photoconductivity (PC) measurements were now applied as a further technique to reveal the influence of varying dislocation densities in combination with ultralow concentrations of chemical impurities on the electronic properties of

06 December 2023 07:12:10

diamond. In order to facilitate a direct comparison, the same sets of systematic samples were employed. In a first step, the chemical impurity data were completed by high sensitivity nitrogen concentration measurements. Then, x-ray induced PC measurements using a laboratory molybdenum (Mo) x-ray tube were performed on all samples. In contrast to the CCE data, which are intrinsically limited to a maximum value of 100% equivalent to the complete collection of all carriers generated by an impinging α -particle, in PC measurements, the current is not limited to a photoconductive gain $G = 1$ (all holes and electrons are simply extracted from the crystal). As a consequence, G values ranging between < 1 and $> 10^4$ were found. These were interpreted in the framework of a recent simulation study on gain formation in diamond.⁵ Finally, also, the settling time behavior after switching the x rays was recorded revealing various levels of persistent photoconductivity (PPC). The observed behavior indicated an indirect contribution of the dislocations.

It turned out that the PC data were strongly dominated by the ratio between boron and nitrogen substitutional impurities, though both were present in ultralow absolute concentrations ≤ 1 ppb. At the same time, the signal height seemed to be completely independent of the dislocation density. Both observations are in complete contrast to the behavior observed in recent CCE measurements. Finally, the present data revealed a pronounced influence of the dislocations on the PC decay time after termination of the x-ray illumination.

II. EXPERIMENTAL

A. Sample preparation

The diamond samples studied in this work were grown heteroepitaxially by MWPCVD on the multilayer substrate Ir/YSZ/Si (001). In a first step, pulsed laser deposition (PLD) was used to grow yttria-stabilized zirconia (YSZ) on 4-in. Si(001) off-axis wafers with a tilt angle of 6° . In the next step, thin iridium films were deposited on top of the YSZ using e-beam evaporation (for details, see Refs. 6 and 7). Then, epitaxial diamond nuclei were created on the Ir surface by bias enhanced nucleation (BEN) at a voltage of about -300 V in a gas mixture of 3% CH_4 in H_2 . In the subsequent growth process, the diamond layers were grown to total thicknesses of 2.2 mm (sample MFAIX394), 4.4 mm (sample MFAIX438), and 1.3 mm (sample MFAIX484). The gas composition was 8% CH_4 in H_2 at a pressure of 150–200 mbar which facilitated growth rates in the range of 10–15 $\mu\text{m}/\text{h}$. Ultrapure hydrogen, obtained by passing the gas through a AgPd membrane, was used for the processes. The purity of the CH_4 process gas was 99.9995%. No nitrogen was added intentionally to the feed gas.

After the deposition, the substrate was completely removed by dissolution of the silicon in KOH solution and by mechanical grinding. 5×5 mm² crystals were cut from the wafers. Then, the highly defective first 5–10 μm were removed on the nucleation side. The two thick samples, i.e., MFAIX394 and MFAIX438, were sliced horizontally by laser cutting into 4 and 8, ≈ 300 μm -thick plates, respectively. The samples exhibit a slight scatter in the absolute thickness (MFAIX394: 312.5 ± 5.6 μm and MFAIX438: 310.2 ± 11.7 μm) with the specific values for each slice listed in the recent work.⁴ All the slices were numbered consecutively

starting with, e.g., MFAIX394_1, for the piece of highest structural quality taken directly at the growth surface and ending with the piece next to the nucleation layer. Only one 560 μm -thick plate was prepared from the growth side of sample MFAIX484. This higher thickness value is taken into consideration during interpretation of the photocurrent data in Sec. IV.

B. Structural data and impurities

For the two thick crystals, various structural data had been acquired in addition to the CCE measurements recently (for details, see Ref. 4). They revealed the decrease of the dislocation density from above 10^9 cm⁻² at a thickness of ≈ 10 μm to $\approx 10^7$ cm⁻² at the growth surface. Simultaneously, the concentration of negatively charged silicon-vacancy defects (SiV^-) as derived from photoluminescence (PL) spectra, which were calibrated by optical absorption measurements, decreased in sample MFAIX394 within the first 200 μm from several ppb to a constant plateau equivalent to 0.7 ppb. In sample MFAIX438, the initial SiV^- concentration of ≈ 1 ppb dropped to few ppt above a thickness of 2 mm.⁴ Since only a minority ($< 15\%$) of the silicon atoms are incorporated as part of SiV related centers,⁸ the absolute silicon concentration should be higher by nearly an order of magnitude. Incorporation was attributed to etching of the Si substrate wafer and the quartz bell jar.

For the electronic behavior of a semiconductor, impurities with donor or acceptor characteristics and the concentration ratio between both are of predominant relevance. In diamond, neutral substitutional nitrogen is known to act as a deep donor (1.7 eV). Since it is the dominant impurity in the feed gas, its concentration has to be known. On the other side, substitutional boron is a relatively shallow acceptor in diamond. It is *a priori* not expected to be found in diamond grown in pristine reactors, which have never been used for boron doping experiments. However, experiments show its omnipresence in CVD crystals at least in the low ppb range.

In this study, the rapid passage electron paramagnetic resonance (RP-EPR) technique is used for determining the concentration of neutral substitutional nitrogen by an experimental setup based on a Bruker E580 EPR spectrometer equipped to an X-band microwave bridge (frequency between 8 and 12 GHz) both in the dark and while excited with above bandgap light. A 224 nm pulsed laser (Photon Systems HeAg70-224SL) is used to illuminate diamond to saturation before each RP-EPR measurement, which maximally neutralizes the positively charged substitutional nitrogen defects, and the laser was kept on during the measurement. The concentrations of defects measured in different conditions are summarized in Table I.

Finally, the substitutional boron concentration N_B was derived from cathodoluminescence (CL) measurements using the T64000 Raman spectrometer (Horiba), a liquid He cryostat (CryoVac), and a 30 keV electron gun (Specs RHEED RHD-30). Measurements were performed at 7.5 K always on several spots using electron energies of 7–8 keV. The intensity ratio between the boron bound exciton $I(\text{BE}^{\text{TO}})$ and the free exciton $I(\text{FE}^{\text{TO}})$ was determined from the spectra and converted into relative concentrations of total

TABLE I. Concentrations of substitutional nitrogen and boron in the studied crystals as derived by EPR or CL, respectively. The EPR data were acquired in the dark and under 224 nm pulsed laser excitation. Samples labeled -A and -B correspond to horizontal slabs, while -C indicates vertical cross section samples. The thickness values of the original wafers were 2.2 mm (MFAIX394), 4.4 mm (MFAIX438), and 1.3 mm (MFAIX484).

Wafer name	Sample name	N_{N^0} dark (ppb)	N_{N^0} UV illuminated (ppb)	N_B (ppb)
MFAIX394	-A	0.50 ± 0.20	0.80 ± 0.20	0.62 ± 0.27
	-B	0.30 ± 0.20	0.98 ± 0.20	
	-C			
MFAIX438	-A	0.17 ± 0.05	0.29 ± 0.10	0.42 ± 0.20
	-B	0.11 ± 0.05	0.11 ± 0.05	
	-C			
MFAIX484	-A	0.15 ± 0.05	0.35 ± 0.10	1.00 ± 0.40

substitutional boron using the equation

$$N_B = 4 \times 10^{16} \frac{I(\text{BE}^{\text{TO}})}{I(\text{FE}^{\text{TO}})} \frac{1}{1.77 \times 10^{23}}. \quad (1)$$

The used calibration constant $(4 \pm 1.7) \times 10^{16}$ was an averaged value from the literature values 2.7×10^{16} at 5 K,⁹ 3.5×10^{16} at 5 K,¹⁰ and 6×10^{16} at 13 K.¹¹ The numerical value 1.77×10^{23} corresponds to the density of diamond given in atoms per cm^3 . Table I shows the deduced values of N_B for the three wafers with the errors comprising scatter of the data measured at different spots and uncertainty from the calibration constant.

C. Electrical measurements

All samples were polished mechanically and oxygen terminated before the deposition of the Ti/Pt/Au (50/20/100 nm) contacts on the two opposing faces by e-beam evaporation. For the subsequent contact annealing, the samples were placed in a sealed quartz ampoule under argon atmosphere. The heat treatment for 2 h at 525 °C was performed to induce carbide formation at the diamond/Ti interface,¹² while Pt/Au protects the Ti against oxidation and facilitates the attachment of bonding wires. Good ohmic behavior is mandatory to guarantee replenishment of holes in the present photocurrent study,¹³ while it was not necessary in the former CCE experiments performed on the identical samples equipped with other contact metals.⁴ The detectors were then mounted in a stainless-steel chamber equipped with a thin diamond window for the entry of the radiation. The chamber was evacuated by a diaphragm pump to avoid parasitic currents from air ionization. X rays were delivered by a standard Mo tube [energy of the characteristic emission line $E(K_{\alpha,1}) = 17.5 \text{ keV}$] usually used for diffraction experiments. In the present experiments, the acceleration voltage and the emission current were set to 50 kV and 20 mA, respectively. Photocurrents were measured by a Keithley 6517B, which also served as a voltage source.

In order to determine the absolute dose rates delivered to the diamond crystals, the soft x-ray chamber type 23342 with an active

volume of 0.02 cm^3 (PTW-Freiburg) was placed at the location of the crystals. Since the soft x-ray chamber had been calibrated in a water dose, the correct diamond dose required multiplication with the ratio between the mass energy absorption coefficients of diamond and water. Instead of diamond, we used the value of graphite from Ref. 14. To vary the dose rate, V, Ni, Zr, and several Ta absorbers of different thickness were placed in the x-ray path.

III. RESULTS

A. Dark conductivity

Figure 1 shows dark conductivity measurements for a selection of samples prepared from the crystals synthesized in three different process runs. The data reveal fundamental and systematic differences.

The dark currents of the four slices cut from crystal MFAIX394 are at the noise level up to the maximum voltage of 300 V for both polarities. Two of the curves are shown in Fig. 1.

In contrast, for the crystal MFAIX438, the maximum currents scatter between 10^{-10} and 10^{-7} A. The asymmetry in the polarity of MFAIX438_1 correlates with highly asymmetric behavior of the same slice in former CCE measurements,⁴ while the reason for the strong dependence on the polarity of MFAIX438_3 is currently unclear.

Finally, the conductivity of sample MFAIX484 is significantly higher ending at 10^{-6} A for 300 V.

In nominally undoped diamond single crystals, increased bulk conductivity at room temperature is typically attributed to some

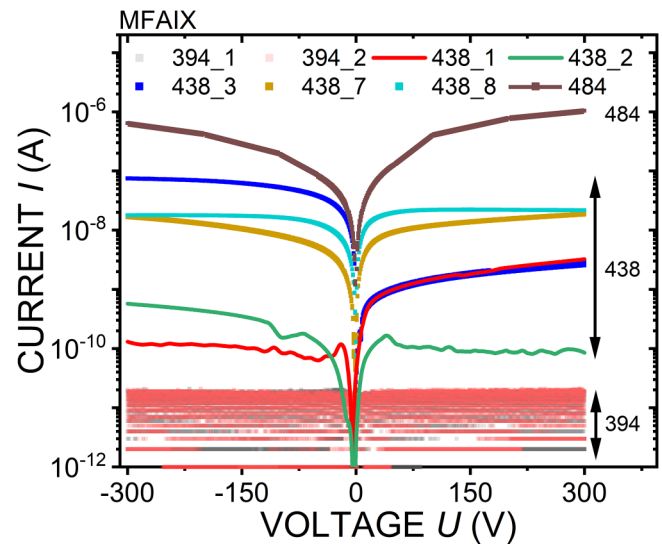


FIG. 1. Dark currents measured for voltages up to 300 V on a selection of detector samples prepared from crystals grown in process runs MFAIX394, MFAIX438, and MFAIX484. The negative voltages were realized by reversing the electrical connections at the crystals. Due to the current limit of the Keithley 6517B, for sample MFAIX484, several data points beyond ± 50 V had to be measured with a different amperemeter separately.

unintentional boron contamination. In consideration of the tolerances for the quantification of nitrogen and boron at absolute levels around 1 ppb by EPR and CL, respectively (see Table 1), the present data can be interpreted as follows: In wafer MFAIX394, the concentration of substitutional nitrogen ($N_N \approx 1$ ppb) is higher than that of boron ($N_B \approx 0.62$ ppb). Boron is fully compensated, and about 40% of the incorporated nitrogen is still left in the neutral charge state. As a consequence, the dark current stays below the noise level ($< 10^{-11}$ A) up to the highest voltages used in the experiment.

For MFAIX438 and MFAIX484, the EPR and CL data do not permit unambiguous conclusions with similar clarity. In both crystals, the concentrations of neutral substitutional nitrogen are detectable but very low (0.1–0.2 ppb) in the dark. Under UV illumination, the positively charged substitutional nitrogen atoms are neutralized, and the concentration of neutral substitutional nitrogen increases to approximately 0.3 ppb (for MFAIX438) and 0.35 ppb (for MFAIX484). This is in both cases below the corresponding concentrations $N_B \approx 0.62$ ppb and $N_B \approx 1.0$ ppb derived by CL. Furthermore, the electrical data showing significantly higher conductivities seem to exclude full compensation specifically for the sample MFAIX484. We, therefore, conclude $N_N \approx N_B$ for MFAIX438 and $N_N < N_B$ for MFAIX484.

B. X-ray radiation induced photoconductivity

In the following photocurrent measurements, all the diamond detectors were exposed to x rays from a Mo tube with a dose rate of 0.073 Gy/s, while the voltage was raised to 300 V in steps of 1 V maintaining a settling time of 3 s per step. Figure 2 summarizes the results with (a), (c), and (e) displaying the data in log-linear plots, while (b), (d), and (f) show the same with two linear axes. Due to the current limit of the voltage source, the measurements for MFAIX484 were stopped at 50 V.

With the e-h pair creation energy $\epsilon_{\text{Dia}} = 13$ eV, the dose rate of 0.073 Gy/s results in an e-h pair creation rate of 1.2×10^{14} cm $^{-3}$ s $^{-1}$. Multiplication with the active volume of the detector crystal, i.e., the irradiated crystal volume between the two electrodes, and with the elementary charge e yields characteristic current I_0 . This current is measured when neither trapping nor carrier injection by the electrodes occurs and all the generated carriers are simply extracted out of the crystal. The photocurrent $I = I_0$ is equivalent to the gain $G = 1$.

As for the dark currents, the photocurrent data split into three different groups with distinct behavior. In the detectors manufactured from crystal MFAIX394, the signals at low voltage (roughly below ± 100 V) are dominated by carrier trapping resulting in $G < 1$. Toward ± 300 V, the four slabs reach photocurrents equivalent to gain values of 3–6. There is no systematic correlation with dislocation density. Instead, the by far highest photocurrents and gain values are obtained for the second slab [MFAIX394_2, red curve in Fig. 2(a) and (b)], while MFAIX394_1, _3, and _4 behave similarly. This is in clear contrast to the CCE data of holes and electrons for this sample series,⁴ which had shown a monotonic decrease with a higher sample number equivalent to higher dislocation density.

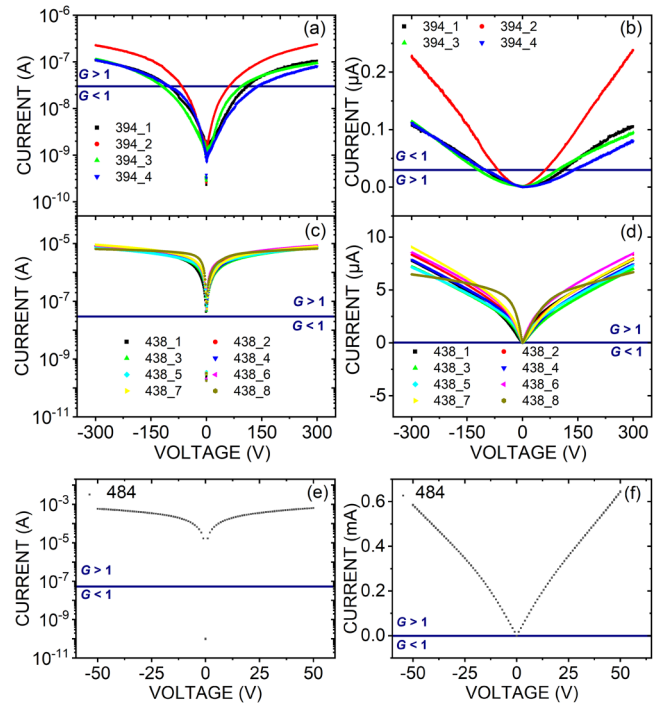


FIG. 2. Photocurrent measurements on all slices of the three crystals under exposure by x rays from a Mo tube with a dose rate of 0.073 Gy/s. The data in (a), (c), and (e) are displayed as semi-logarithmic plots and in (b), (d), and (f) as linear plots. The horizontal lines indicate the photocurrent I_0 corresponding to $G = 1$.

In the eight detectors manufactured from crystal MFAIX438, the photocurrent is above I_0 virtually over the whole range of applied bias voltages. At ± 300 V, maximum values equivalent to $G \approx 300$ are obtained. The curves in Figs. 2(c) and 2(d) show a similar basic shape except for MFAIX438_8, the detector prepared from the crystal region closest to the nucleation zone with the highest dislocation density. Again, there is no systematic variation with n_{dis} in contrast to the former CCE data, which had shown the trend of increasing collection efficiency for holes with decreasing dislocation density. Collection of electrons was generally weak in this sample series.

Finally, the detector MFAIX484 yields a current of about 0.6 mA already at ± 50 V equivalent to $G \approx 7500$.

Comparison between the three sets of samples facilitates the first conclusion that high dark conductivity is correlated with high photoconductive gain under x-ray exposure.

For a further discussion, we analyzed the curve shape in the low field region. Figures 3(a)–3(c) show the photocurrents in the field range of 0–0.12 V/ μm compared with the field dependence of the hole drift velocity taken from Berdermann¹⁵ based on the work of Pomorski.¹⁶

The photocurrent of MFAIX394_2 shows a superlinear increase, i.e., a positive curvature. Due to $G < 1$, charge transport is dominated by trapping of the charge carriers created by the

x rays (holes and electrons) resulting in space charges within the crystal and a nonlinear characteristic line shape. In contrast, the curve shape of the photocurrent measured for MFAIX438_5 nicely fits the field dependence of the hole drift velocity. The finding of $G > 1$ means that the current is predominantly due to transport of holes, which are injected via the anode, then transit the whole

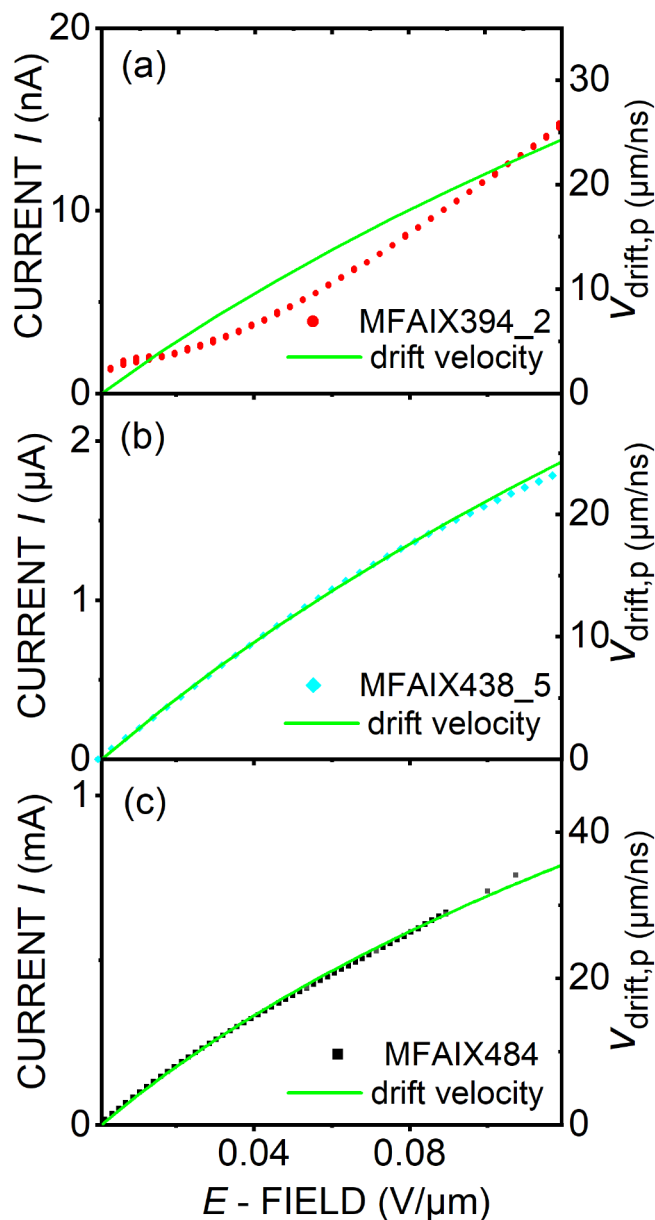


FIG. 3. Comparison between the curve shape of the measured photocurrents (dots) and the field dependence of the hole drift velocity taken from the literature (green line) for always one exemplary detector sample fabricated from (a) MFAIX394, (b) MFAIX438, and (c) MFAIX484. Dose rate: 0.073 Gy/s.

crystal, and finally leave it via the cathode. The negative curvature is a consequence of the beginning saturation of the drift velocity equivalent to a decrease in mobility. This also holds for MFAIX484 up to 0.1 V/μm. Above this value, the current rises rapidly. The identical development of the photocurrent and the drift velocity with increasing field strength is compatible with the model of a homogeneous hole carrier density within the diamond detector volume as assumed for our model on the formation of photoconductive gain.⁵ The results suggest the validity of this assumption in the range of low fields for crystals MFAIX438 and MFAIX484, but definitely not for MFAIX394.

C. The settling time behavior

The time the photocurrent needs to reach a constant value after switch-on and especially the decay time that is required to return to the original dark current level at the end of the irradiation are technologically relevant detector parameters in dosimetry applications. In addition, the settling time behavior can yield valuable information on the involved traps. It is compared for all detectors in Fig. 4. For the detectors manufactured from MFAIX394 and MFAIX438, the applied field strength was 0.2 V/μm identical to the value used in our former calculations.⁵ For MFAIX484, it was reduced to 0.1 V/μm.

In Fig. 4(a), for all four detectors of crystal MFAIX394, the current increases by more than 3 orders of magnitude within a few seconds. In agreement with measurements in Fig. 2(b), the absolute value for MFAIX394_2 (red curve) is higher by a factor of ≈ 2.5 . After switching off the x rays, the decay by 1 and 2 orders of magnitude occurs within ≈ 1 s and 8.8 ± 8 s, respectively. After 1 h, all the detectors have reached a common level of $2.5(\pm 0.5) \times 10^{-11}$ A, while total decay by 3 orders of magnitude is not reached within the measurement time (2h). No correlation of the decay time or the level of the PPC with the dislocation density is found for this set of samples.

The eight detectors of crystal MFAIX438 show a comparatively homogeneous turn-on to a photocurrent of $2.3(\pm 0.77) \times 10^{-6}$ A. After switch-off, the decrease by 1 and 2 orders of magnitude requires 24–1600 s and 560–60 000 s, respectively. The great range in the absolute values is not due to a statistical scatter. Instead, there is a clear trend that the decay slows down, and the PPC values increase with dislocation density n_{dis} (see Fig. 5).

In the final sample MFAIX484, the time for the decrease after switch-off by 1 and 2 orders of magnitude has further increased to 1900 s and 91 000 s, respectively.

IV. DISCUSSION

In the present study, x-ray induced photoconductivity data have been measured, and experimental gain values G have been derived for three sets of heteroepitaxial diamond samples in which (i) the dislocation density varied systematically from $\approx 10^7$ up to $\approx 10^9$ cm⁻² for two sample series and (ii) which showed pronounced differences in dark conductivity. All the crystals were of very high purity with both nitrogen and boron in the narrow range between 0.1 and 1.0 ppb.

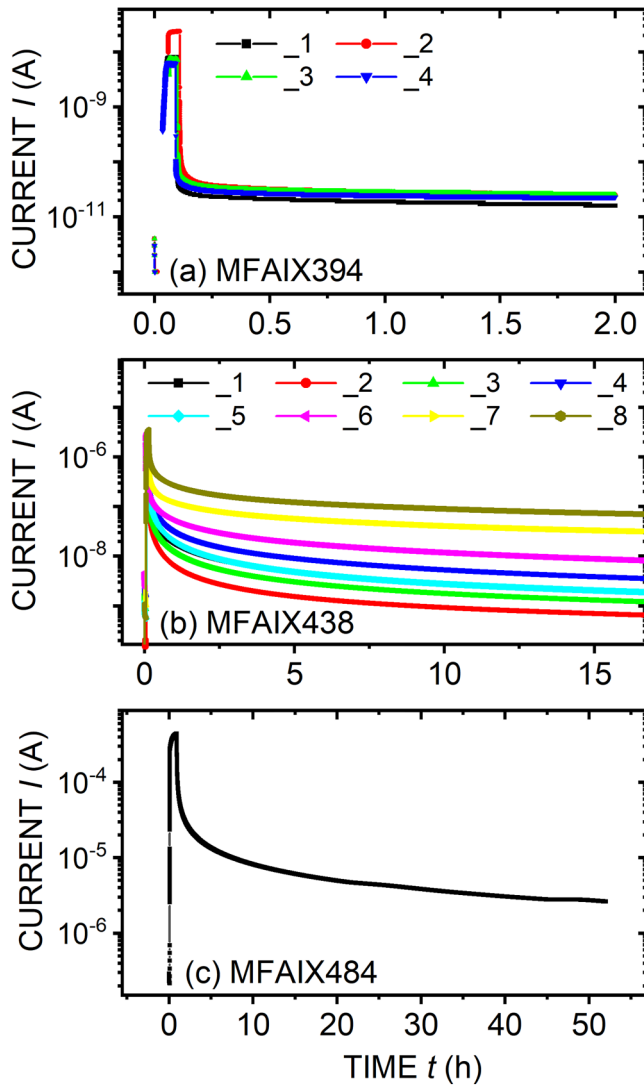


FIG. 4. Settling time behavior measured for all prepared detector samples: (a) MFAIX394, (b) MFAIX438, and (c) MFAIX484. The field strength was 0.2 V/μm in (a) and (b) and 0.1 V/μm in the case of (c). Dose rate: 0.073 Gy/s.

As a first observation, we note drastic differences in dark conductivity. The curves can be assorted into three groups: the four detectors prepared from MFAIX394 with currents below the noise level of $< 10^{-11}$ A, the eight detectors from MFAIX438 with dark currents at 300 V scattering between 10^{-10} and nearly 10^{-7} A, and finally the detector MFAIX484 with a maximum current of 10^{-6} A. Attributing the conductivity to free holes released from boron acceptors, we conclude in accordance with EPR and CL data presented in Table I that in the first group, the boron is well compensated by nitrogen, $N_N > N_B$, in the second group $N_N \approx N_B$, and finally $N_N < N_B$ for sample MFAIX484.

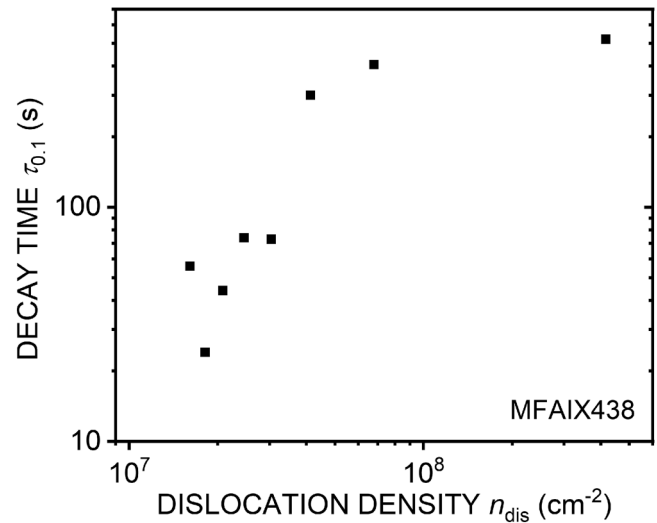


FIG. 5. Time required for the decay of the photocurrent by one order of magnitude after x-ray irradiation switch-off vs dislocation density n_{dis} . The data points were derived for the eight samples of crystal MFAIX438 from the currents shown in Fig. 4 (b).

At 0.2 V/μm, the photocurrent measurements in Figs. 2(a)–2(d) yield $G = 0.53 \pm 0.34$ and $G = 97 \pm 15$ for the detectors fabricated from MFAIX394 and MFAIX438, respectively. According to our model, these gain values would require $N_N = 420$ and 3.7 ppb, respectively. While the 3.7 ppb for MFAIX438 is of a reasonable size (on the order of unity), the value of 420 ppb for MFAIX394 is unrealistically high.

The value of G for the third crystal MFAIX484 exceeds the gain of the other two sample series by several orders of magnitude, though its boron concentration is not more than by a factor of two higher and the nitrogen concentration is similar to that of MFAIX438. With $N_N < N_B$, i.e., $R = (N_N - N_B)/N_B < 0$, the value of $G = 1.2 \times 10^4$ predicted by our simulation for $E = 0.1$ V/μm and $R \approx 0$ compares reasonably well with the experimental result of $G = 0.75 \times 10^4$. In this comparison, the higher thickness (560 μm) of sample MFAIX484 is taken into consideration.

These findings suggest that our model is best applicable for low (or slightly negative) compensation ratios R yielding high gain values, while it shows strongest deviations for low G values in defect-rich crystals. We attribute this observation to the different role that additional traps, such as dislocations or point defects like vacancies or silicon containing defects, play in high and low gain samples. As shown in former CCE measurements,⁴ deep hole trapping is not ignorable in all crystals but specifically not in the detectors from MFAIX394. The responsible traps may be filled quickly by the high hole currents typical for MFAIX438 and MFAIX484. This process causes little changes in the absolute current. In contrast, in MFAIX394, the competition between filling and emptying results in a pronounced permanent influence of the traps on the absolute PC. As a consequence, the current is much lower than predicted by the computer simulation, which worked without additional traps.

06 December 2023 07:12:10

The studied settling time behavior first of all yields a clear correlation between high gain and slow decay. This is a general trend for many types of detectors from different solid materials.¹⁷ Moreover, the data for the sample series MFAIX438 also show a pronounced influence of the dislocations: the higher the dislocation density, the slower the decay (see Fig. 5). This is remarkable since neither in the dark current nor in the absolute height of the photocurrents, dislocations virtually played any role.

The decay of this PPC can be analyzed in the highest gain sample MFAIX484 [see Fig. 4(c)] in the following way by considering only the role of B and N: The concentrations of boron and nitrogen in this sample are $N_B = 1 \text{ ppb} = 1.77 \times 10^{14} \text{ cm}^{-3}$ and $N_N = (1 - \delta)N_B$. With the use of “ δ ,” we take into account that the surplus of boron with respect to nitrogen is expected to be small. After x-ray turn-off, the low electron current ($< 0.1\%$) will disappear immediately due to extraction from the crystal or capturing inside by N^+ . Thus, only hole currents have to be considered. These holes can be captured by B^- , N^0 or they are thermally released from the B^0 into the valence band. The time constant for thermal excitation of holes from B acceptor levels is 160 ns.⁴ With $N_{B^-} \approx N_B$, the lifetime of the holes in the valence band due to capture by B^- can be estimated to

$$\tau_p = \frac{1}{\sigma_{B^-} v_{th,p} N_{B^-}} = 2.1 \times 10^{-9} \text{ s} \approx 2 \text{ ns.} \quad (2)$$

In this calculation, the values for the capture cross section σ_{B^-} and the thermal velocity of holes $v_{th,p}$ are $1.8 \times 10^{-13} \text{ cm}^2$ and $1.5 \times 10^7 \text{ cm/s}$, respectively.⁵ Due to the lower concentration of N^0 and $\approx 2 \times 10^3$ times smaller capture cross section of neutral atoms,⁵ trapping events by N^0 are several orders of magnitude rarer. As a consequence, there is an equilibrium between free holes and B^0 , which establishes a quasi-Fermi level for holes in the valence band. It is described by the mass action law,

$$v_{th,p} \sigma_{B^-} p N_{B^-} = \frac{1}{\tau_B} N_{B^0}. \quad (3)$$

The maximum current $I(t)$ in Fig. 4(c) is in the range of several times 10^{-4} A and the corresponding hole density p ,

$$p = \frac{Id}{eVv_{drift,p}}. \quad (4)$$

With a hole drift velocity of $v_{drift,p} = 2.1 \times 10^6 \text{ cm/s}$ at $0.1 \text{ V}/\mu\text{m}$, a detector thickness $d = 0.056 \text{ cm}$, the active detector volume of $V = 2.75 \times 10^{-3} \text{ cm}^3$, and the current of $1 \times 10^{-4} \text{ A}$ as obtained 351 s after switch-off yields a hole density of $p = 6.05 \times 10^9 \text{ cm}^{-3}$. The sum of free holes and holes trapped at boron atoms is

$$p_{total} = p + N_{B^0}. \quad (5)$$

With $C_2 = \frac{1}{\tau_B v_{th,p} \sigma_{B^-}}$, the combination of (3) and (5) yields

$$p_{total} = p + N_{B^0} = p + \frac{p N_B}{p + C_2} = \frac{p}{p + C_2} (p + C_2 + N_B). \quad (6)$$

With $C_2 = 2.31 \times 10^{12} \text{ cm}^{-3}$ and $N_B = 1.77 \times 10^{14} \text{ cm}^{-3}$, Eq. (6) can be approximated by

$$p_{total} \approx p \frac{N_B}{C_2} \quad (7)$$

and also

$$\dot{p}_{total} \approx \dot{p} \frac{N_B}{C_2}. \quad (8)$$

Capture of holes by N^0 is a small perturbation to the hole equilibrium at the valence band. It is responsible for the slow but monotonic decrease of the PPC. The resulting dynamics can be described by

$$\dot{p}_{total}(t) = p(t) v_{th,p} \sigma_{N^0,eff} N_{N^0}. \quad (9)$$

Combining (8) and (9), one can derive the capture cross section of N^0 for holes,

$$\sigma_{N^0,eff} = \frac{\dot{p}(t) \frac{N_B}{C_2}}{p(t) v_{th,p} N_{N^0}}. \quad (10)$$

From $N_N = (1 - \delta)N_B$, charge neutrality requires $N_{N^0} = N_{N^0}(t) = p_{total}(t) - \delta N_B \approx p(t) \frac{N_B}{C_2}$ so that we obtain

$$\sigma_{N^0,eff} = \frac{\dot{p}(t)}{p^2(t) v_{th,p}} = \frac{eV v_{drift,p} \dot{I}(t)}{d v_{th,p} I^2(t)}, \quad (11)$$

where $\sigma_{N^0,eff}$ is plotted in Fig. 6.

Figure 6 shows an initial cross section of 10^{-19} cm^2 , which decreases first rapidly and then slowly to $4 \times 10^{-21} \text{ cm}^2$ after 2 h. All these values are well below the 10^{-16} cm^2 reported for hole capture by neutral nitrogen.¹⁸

Such a huge reduction by a factor 10^4 could be due to an energetic barrier the holes have to cross in order to reach the neutral nitrogen atoms. For a cross section of 10^{-20} cm^2 , a height $\Delta E = 0.24 \text{ eV}$ can be estimated from the relationship

$$e^{\frac{\Delta E}{k_B T}} = 1 \times 10^4. \quad (12)$$

The barrier can be created by the stress field around dislocations. A small fraction of nitrogen atoms located in regions with downward bending of the valence band edge exhibit this barrier with the exact height depending on position and distance from the dislocation core.⁴ The higher the barrier, the later the corresponding atoms will be recharged by capturing a hole. As a consequence, the effective cross section of all the remaining nitrogen atoms decreases monotonically with time. At a PPC of 10^{-4} A , the fraction of uncharged high-barrier nitrogen atoms amounts to 0.26% according to these considerations.

Furthermore, this small fraction also yields the crucial key information to understand the intriguing difference in behavior of the MFAIX394 samples in the previous CCE measurements and in the present PC study: While MFAIX394 had shown the most

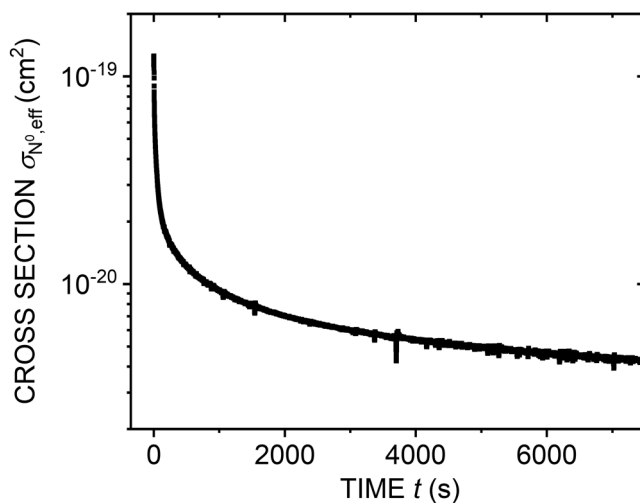


FIG. 6. The cross section $\sigma_{N^0,eff}$ for hole capture by neutral nitrogen derived by application of Eq. (11) to the $I(t)$ curve in Fig. 4(c) plotted vs the time after x-ray switch-off.

pronounced correlation with dislocation density in the CCE data, here, dislocations are virtually irrelevant for the PC and decay time. This is simply due to the fact that the high excess of nitrogen always guarantees that sufficient high cross section nitrogen is present to capture the free holes. Nitrogen atoms located close to the dislocation cores do not play a role.

V. SUMMARY

The photoconductivity under x-ray irradiation has been studied for one individual crystal and two sets of heteroepitaxial diamond samples with a systematic variation of the dislocation density. All the crystals were of very high purity with both nitrogen and boron concentrations, in the narrow range of 0.1–1.0 ppb as measured by EPR and CL. Though grown by MWPCVD under nominally identical conditions, their dark currents varied drastically ranging from $\leq 10^{-11}$ A up to 10^{-6} A. The photocurrents showed a similar broad variation with a photoconductive gain G of 0.53 (at 0.2 V/ μ m) up to 0.75×10^4 (at 0.1 V/ μ m). As a first clear trend, a positive correlation between high dark conductivity and high photocurrent was revealed. Differences in dark as well as photoconductivity can be explained by different compensation of boron acceptors by nitrogen donors. The measured gain and the G value predicted by our former model show a reasonable agreement for the high gain samples. The low gain samples would require unreasonably high nitrogen concentrations to explain their behavior in the framework of our model. These deviations are easily comprehensible by the fact that the low detector currents are strongly controlled by trapping, which means a dominating influence of additional electronically active defects in addition to N and B.

The settling time of the photocurrents is short for the low gain crystal. In the high gain crystals MFAIX438 and MFAIX484, the slow decay and the high PPC are attributed to an energy

barrier for the capture of free holes by neutral nitrogen atoms. A small fraction of substitutional nitrogen atoms resides in an environment that generates this barrier. As a plausible source, the stress fields around dislocation causing downward bending of the valence band edge are suggested. The correlation between the dislocation density and the slower decay in the samples of crystal MFAIX438 supports this idea. Further investigations are desirable to corroborate this model and reveal possible contributions of additional chemical defects, such as silicon related centers and electronic levels generated by dislocations.

ACKNOWLEDGMENTS

We gratefully acknowledge financial support by the GSI Helmholtzzentrum für Schwerionenforschung and by the German Research Foundation DFG (No. SCHR 479/5-1, 411398861). We would also like to thank PTW-Freiburg Physikalisch-Technische Werkstätten Dr. Pychlau GmbH for the temporary lending of a dosimeter for photoconductivity measurements, Michael Träger (GSI Darmstadt) for conductivity measurements, Dr. Martin Fischer and Dr. Stefan Gsell for crystal growth, and Dr. Michael Mayr for some sample preparation. MEN acknowledges funding from the EPSRC (EP/V056778/1 and EP/T001062/1) and JZ from the University of Warwick.

AUTHOR DECLARATIONS

Conflict of Interest

The authors have no conflicts to disclose.

Author Contributions

T. Grünwald: Investigation (lead); Writing – review & editing (supporting). **C. Bestele:** Data curation (equal); Investigation (equal). **M. Bosak:** Data curation (supporting). **J. Zhao:** Data curation (equal); Investigation (equal). **M. E. Newton:** Formal analysis (equal); Writing – review & editing (equal). **M. Schreck:** Conceptualization (lead); Data curation (equal); Formal analysis (equal); Funding acquisition (lead); Project administration (lead); Writing – original draft (lead).

DATA AVAILABILITY

The data that support the findings of this study are available within the article.

REFERENCES

- ¹M. Prelas, G. Popovici, and L. Bigelow, *Handbook of Industrial Diamonds and Diamond Films* (Routledge, 1998).
- ²D. Kramer, *Phys. Today* **75**(3), 22 (2022).
- ³M. Schreck, S. Gsell, R. Brescia, and M. Fischer, *Sci. Rep.* **7**(1), 44462 (2017).
- ⁴M. Schreck, P. Ščajev, M. Träger, M. Mayr, T. Grünwald, M. Fischer, and S. Gsell, *J. Appl. Phys.* **127**(12), 125102 (2020).
- ⁵T. Grünwald and M. Schreck, *J. Appl. Phys.* **129**(12), 124502 (2021).
- ⁶S. Gsell, T. Bauer, J. Goldfuß, M. Schreck, and B. Stritzker, *Appl. Phys. Lett.* **84**(22), 4541 (2004).
- ⁷S. Gsell, M. Fischer, T. Bauer, M. Schreck, and B. Stritzker, *Diam. Relat. Mater.* **15**(4–8), 479 (2006).

- ⁸U. D'Haenens-Johansson, A. Edmonds, B. Green, M. Newton, G. Davies, P. Martineau, R. Khan, and D. Twitchen, *Phys. Rev. B* **84**(24), 245208 (2011).
- ⁹J. Barjon, *Phys. Status Solidi A* **214**(11), 1700402 (2017).
- ¹⁰F. Omnès, P. Muret, P.-N. Volpe, M. Wade, J. Pernot, and F. Jomard, *Diam. Relat. Mater.* **20**(7), 912 (2011).
- ¹¹M. Kasu, M. Kubovic, A. Aleksov, N. Teofilov, Y. Taniyasu, R. Sauer, E. Kohn, T. Makimoto, and N. Kobayashi, *Diam. Relat. Mater.* **13**(2), 226 (2004).
- ¹²S. Koizumi, H. Umezawa, J. Pernot, and M. Suzuki, in *Power Electronics Device Applications of Diamond Semiconductors*, Woodhead Publishing Series in Electronic and Optical Materials (Woodhead Publishing, 2018), pp. 219–294; see <https://www.sciencedirect.com/science/article/pii/B9780081021835000042>.
- ¹³R. H. Bube, *Photoconductivity of Solids* (New York, John Wiley & Sons, 1960).
- ¹⁴J. Hubbell and S. M. Seltzer, *X-Ray Mass Attenuation Coefficients* (National Institute of Standards and Technology, Gaithersburg, MD, 2004), available at <http://physics.nist.gov/PhysRefData/XrayMassCoef/cover.html>.
- ¹⁵E. Berdermann, *Comprehensive Hard Materials* (Oxford, Elsevier, 2014), pp. 407–467.
- ¹⁶M. Pomorski, “Electronic properties of single crystal CVD diamond and its suitability for particle detection in hadron physics experiments,” Ph.D. thesis, Wolfgang von Goethe Universität, Frankfurt am Main, 2008.
- ¹⁷C. Xie, X.-T. Lu, X.-W. Tong, Z.-X. Zhang, F.-X. Liang, L. Liang, L.-B. Luo, and Y.-C. Wu, *Adv. Funct. Mater.* **29**(9), 1806006 (2019).
- ¹⁸L. S. Pan, D. Kania, P. Pianetta, J. Ager III, M. Landstrass, and S. Han, *J. Appl. Phys.* **73**(6), 2888 (1993).